SOLUTION OF THREE-DIMENSIONAL SUPERSONIC FLOWFIELDS VIA ADAPTING UNSTRUCTURED MESHES

Todd J. Mitty, Antony Jameson and Timothy J. Baker
Department of Mechanical and Aerospace Engineering, Princeton University, Princeton, New Jersey 08544 USA

ABSTRACT

Adaptive mesh refinement in three-dimensions on unstructured meshes was used to solve the Euler Equations for two supersonic flows. One case was uniform flow past a ramp within a channel — producing a shock wave and its reflection off of a wall of the channel. The other case incorporated a similar geometry, but had a supersonic inviscid vortical sub-layer as an inflow condition. The resultant flow for this case was characteristic of swept shock wave/boundary layer interaction phenomena.

INTRODUCTION

Given a well-posed numerical problem, a suitable computational mesh, a consistent and stable numerical method, and appropriate and consistent numerical boundary conditions, a satisfactory numerical solution should be attainable if the discretization properly resolves important features of the solution. That is, the mesh resolution must be sufficient to maintain the error of the calculation at, or below, some required limit. By using a sufficiently fine mesh, it should be possible to meet this criterion. However, such an option is not always viable since the resolution required to capture certain encountered phenomena within a domain may be beyond the capability of one's computational facility. If the entire domain demands such a resolution for an accurate solution, then this dilemma is unavoidable without either modifying the problem or satisfying oneself with a degradation in flow features (which may or may not affect the overall nature of the solution). Recourse may be taken if only specific locations within the computational domain require a greater discrete resolution. Adaptive mesh alteration is a process which adjusts the computational mesh during progression of the solution to form a mesh more apt to resolve incumbent phenomena of interest. The ultimate goal of adaptive methods is to aid in achieving accurate numerical solutions by economizing both computer memory and computational requirements [1].

In general, adaptive resolution may occur at any arbitrary location within the computational domain. Unstructured meshes, by their very nature, are well suited for such a scenario. Additionally, unstructured meshes allow for rendering of complex geometries. In this work, three-dimensional unstructured meshes were generated by a Delaunay tessellation [2] for geometries of the type in Fig. 1. These meshes were then used to solve two specific supersonic flows — an inlet with uniform flow, and an inlet with a rotational sub-layer. As the solution of these flows progressed, adaptive mesh alteration was enstated to yield improved results over those of the initial mesh.

Unstructured meshes lack contiguity between their data structure and the structured array addressing of current computer languages and architectures. As a result, special array addressing techniques must be incorporated into both the mesh generator and flow solver. In this work, the three-dimensional mesh adaption is performed by the code *MAESTRO*, which interfaces between the mesh generator, *MESHPLANE*, and flow solver, *FLOPLANE*, from Jameson and Baker's *AIRPLANE* code [3].

DISCRETIZATION OF THE DOMAIN

The manner in which one tessellates a given domain is essentially left to choice. However, it is important that the method used be capable of: correctly rendering boundaries of the computational domain; be robust enough to cope with a variety of geometries; and it should be fast and efficient to execute. The type of unstructured mesh most frequently used is a tetrahedral tessellation. Two popular schemes for producing this type of mesh are the "advancing-front" [4] and the Delaunay [2] tessellations.

The Delaunay tessellation of the computational space is obtained by applying Bowyer's Algorithm — which may be stated as [2]:

> *Given a set V_n of n-points in k-space, the Delaunay tessellation is the tessellation of V_n such that no point $P_i \in V_n$ lies inside the circumsphere of any k-simplex.*

In terms of adaptive refinement, the Delaunay tessellation has certain advantages. Perhaps most important being that its application affects the mesh *locally*. Points inserted at *arbitrary* locations within the unstructured computational space will naturally be accepted into the existing tessellation. Additionally, the resultant mesh modification does not obligate a re-meshing of the entire computational space.

Boundary Adaption

At a boundary of the computational domain, one loses the freedom of arbitrary point placement since any point to be added there must fall at a location consistent with the physical boundary. If the boundary can be defined analytically, then the problem of proper modification is somewhat alleviated. In this work, the problem was obviated since the generic geometry was formed from a combination of planes (c.f., Fig. 1), and simple rules could be enforced to ensure proper boundary alteration.

MATHEMATICAL MODEL AND NUMERICAL DESCRIPTION

The Euler Equations provide a mathematical model for the flow of an inviscid compressible fluid. In their integral conservation form they may be drafted as follows for a domain Ω with bounding surfaces $\partial\Omega$,

$$\frac{\partial}{\partial t}\iiint_{\Omega} \mathbf{w}\, d\Omega + \iint_{\partial\Omega} \mathbf{F}\,\mathbf{n}\, d\partial\Omega = 0, \tag{1}$$

where $\mathbf{w}$ is a vector of dependent variables; $\mathbf{F}$ is a flux matrix; and $\mathbf{n}$ is a surface unit normal. These quantities are defined as:

$$\mathbf{w} = \begin{Bmatrix} \rho \\ \rho u \\ \rho v \\ \rho w \\ \rho e_o \end{Bmatrix}, \quad \mathbf{F} = \begin{bmatrix} \rho u & \rho v & \rho w \\ \rho u^2 + p & \rho v u & \rho w u \\ \rho u v & \rho v^2 + p & \rho w v \\ \rho u w & \rho v w & \rho w^2 + p \\ \rho u h_o & \rho v h_o & \rho w h_o \end{bmatrix}, \quad \mathbf{n} = \begin{Bmatrix} n_x \\ n_y \\ n_z \end{Bmatrix},$$

where the primative variables ρ, p, e_o, h_o, u, v, and w are the thermodynamic density, pressure, total specific internal energy, and total specific enthalpy, and three Cartesian velocity components respectively. Furthermore, restricting our analysis to that of a perfect gas, the equation of state is (γ is the ratio of specific heats)

$$e_o = \frac{p}{(\gamma - 1)\rho} + \frac{1}{2}\left(u^2 + v^2 + w^2\right). \tag{2}$$

Equations 1 and 2 form a closed set which may be used to solve for $\mathbf{w}$. Invoking Galerkin's Method (c.f., Jameson and Baker [3]), these equations may be discretized into the familiar unsteady flux residual equation

$$\frac{d}{dt}\left[\left(\sum_k \Omega_k\right)\mathbf{w}_i\right] + \sum_k \left(\tilde{\mathbf{F}}\mathbf{n}\partial\Omega\right)_k = 0, \qquad \tilde{\mathbf{F}} = \frac{1}{3}\left(\mathbf{F}_1 + \mathbf{F}_2 + \mathbf{F}_3\right). \tag{3}$$

The sums in Eq. 3 are over all tetrahedra which meet at a common node i to form a control volume surrounding that node. $\tilde{\mathbf{F}}$ is the average of the flux matrix from the three nodes which form the face of the tetrahedra on the bounding control surface with $\mathbf{n}$ as the normal of that plane. Equation 3 is directly interpretable as a finite volume approximation of the conservation laws (Eq. 1). It may be cast as a first-order ordinary differential equation in time to yield

$$\frac{d\mathbf{w}_i}{dt} + \mathcal{R}(\mathbf{w}_i) = 0, \tag{4}$$

where $\mathcal{R}(\mathbf{w}_i)$ represents a numerical flux-residual at node i.

Numerical dissipation must be added to this discrete approximation for the purpose of removing undamped and/or lightly damped error modes, as well as to prevent solution oscillation near large gradients (e.g., shock waves). Reference [3] presents the form of these dissipative terms which will be stated here as a dissipative residual $\mathcal{D}(\mathbf{w}_i)$, and is lumped with $\mathcal{R}(\mathbf{w}_i)$.

A Runge-Kutta multi-stage explicit time-stepping scheme is used to integrate Eq. 4 (with dissipation included) forward in time. Only the steady state of flows are considered here, and it follows that convergence is attained when the unsteady term in Eq. 4 approaches zero. In this work, a five-stage time-stepping scheme with three evaluations of dissipation per time-step was employed.

TEST CASES

Oblique Shock Wave with Reflection

As a means of benchmarking the adaption scheme, a uniform supersonic Mach 2 flow inlet condition for the geometry of Fig. 1 with a ramp angle of 10° was calculated. The initial coarse mesh (c.f., Fig. 2) contained 1,701 points. The following methodology was used to adaptively alter the mesh: After a specified number of numerical time-steps, the computational domain is swept by two adaption sensors. On each tetrahedral face, an average pressure and an average density is calculated based upon the three nodes which define the face. An absolute percentage change at each of these three nodes from each of the two averages is then calculated. If any of these values exceed some threshold, then that face is refined in the following manner:

- Point addition at the centroid (the arithmetic average of the positions of the forming nodes) of the face.
- Point addition at the midpoint of edge(s) which form the intersection between two bounding surface-planes.

The degree to which a given domain may be refined is essentially only limited by available computer memory, speed, and *precision*. Applying a refinement routine several times will generate successively smaller computational elements with the effect of an increase in mesh resolution, but a decrease in the maximum allowable time-step for an explicit scheme will also result. Jameson [5] has shown that equations of the type in Eq. 4 may be solved with *implicit* time-stepping by using multigrid methods. Additionally, Mavriplis [6] has reported success with a multigrid approach on unstructured meshes in three-dimensions. Thus, it seems possible that this explicit time-stepping constraint, which could inhibit adaptive flow solutions, may be weakened.

Three levels of mesh adaption were applied to the reflecting shock case. A total of 150,999 mesh points were in the final mesh (c.f., Fig. 3). This number is somewhat deceiving since the flow being calculated is uniform in the z-direction. In effect, the computational domain could have been contracted in the z-direction without affecting the flow solution, and the total number of points would subsequently be much less.

The variation in pressure coefficient along a line in the x-direction for the initial and final mesh is plotted in Fig. 4. It is clear that there has been a significant improvement in the flow solution as a result of the adaptation.

Swept Shock/Boundary Layer Problem

The initial impetus for this work was to attempt to solve the flow of a swept shock/boundary layer interaction by means of an inviscid method. It was felt that perhaps the vorticity of the flow governed the primary nature of the flowfield rather that the viscosity and/or turbulence. There has been a great deal of both experimental and computational research over the past 15 years on swept shock/boundary layer interactions [7], and Knight and Horstman have computed many of these flows using the Navier-Stokes Equations with a turbulence model.

The characteristic features of swept shock/boundary layer flow are driven by the presence of an incoming supersonic turbulent boundary layer profile in u-velocity extending in the z-direction (c.f., Fig. 1). As this flow interacts with the compression corner (ramp), the rotational sub-layer rolls up and develops into a vortical structure. Away from the sub-layer exists the shock wave of the two-dimensional "inviscid" region (c.f., Fig. 5). It should be noted that this flow has been shown to be inherently unsteady. However, even the most recent computations of these flows have been steady state solutions [8] — the hypothesis being that one is solving for the mean quantities of flow variables. This assumption will also be made here, although its validity is recognized to be questionable.

As Knight [8] points out, the flowfield is essentially rotational and inviscid except for a very thin region near the wall. The Euler Equations govern the flow of an *inviscid* fluid, and they permit the presence of *vorticity*. It can be argued that these equations are capable of resolving the primary features of the flowfield. For a steady, inviscid, homenergetic flow, Crocco's Equation becomes $\mathbf{\Omega} \times \mathbf{V} = T\nabla s$, where $\mathbf{\Omega}$, $\mathbf{V}$, T, and s are respectively the vorticity vector, velocity vector, temperature and entropy. A typical mechanism for vorticity generation in such a flow would be a shock wave which creates an entropy gradient (i.e, a curved shock). If an inflow boundary condition supplied an *inviscid rotational* flowfield, this vorticity would some how be convected and altered.

The boundary conditions used in this work for computing such a flow are as follows: The entire bounding surface, with the exception of the inlet and exit planes (c.f., Fig. 1), were treated as solid walls with zero normal-flux, but slip was allowed. Since the flow normal to the exit plane was essentially completely supersonic, a one-sided numerical scheme was used there. The inflow condition was a boundary layer profile computed by Knight — with some slight modifications made to conform to the requirements for Euler flow. The v and w-velocity components were both made zero. From the computed profile, $u(z)$ was interpolated at desired locations. Requiring that the flow be homenergetic, $\frac{\partial h_o}{\partial t} = \nabla h_o = 0$, density would be calculated and pressure would then have to be set equal

to its freestream value. The value of the profile at which $u = 0.99u_\infty$ defined the the sub-layer thickness δ_∞, which was subsequently used to non-dimensionalize lengths. This inflow condition provided the initial vorticity of the flow.

Adaptive mesh computations were begun on an initial mesh of 3,751 points as shown in Fig. 6. The wedge angle was 20° and the freestream Mach was 2.935 (inorder to match the computations and experiments of Knight and Bogdonoff [9]). It was necessary to cluster points in the region of the rotational sub-layer inorder to maintain the characteristic sub-layer profile. If this was not done, the artificial dissipation would have flattened the profile greatly. (It is recognized that the artificial viscosity does generate some level of vorticity. By clustering the mesh, it is hoped that the level of this vorticity addition is small. However, this is a topic which will require further investigation.)

Adaption was made in a similar manner to that used in the reflecting shock case with some modifications. If any region in or near the clustered sub-layer was to be adapted, a collection of points distributed on a line normal to the wall in the xy-plane were added. Such a procedure would uphold the integrity of the stretched computational elements in the clustered zone so that the nature of the profile would be maintained.

The computational mesh after three levels of refinement contained 89,155 points and is shown in Fig. 7. The method's ability to capture the "inviscid" shock wave and adapt in the region of the vortical structure can be seen. A comparison of these results with the computational results of Knight and the experimental results of Bogdonoff [9] is given in Figs. 8 to 12

CONCLUSIONS AND FUTURE WORK

The usefulness of the adaption scheme is evident from the results presented. It is recognized that there may be certain flow features that are not well sensed by the adaptive criteria presently being used. A more appropriate set of sensors might be a measure of the discretization error. It is felt that the artificial dissipation may provide such a measure, and this matter is currently being pursued. The results of the shock wave/boundary layer interaction flow indicate that inviscid effects dominate the nature of the global flow. The inviscid computations presented here should be extended to the recent computations and experiments conducted at Mach 4 by Knight [8] and Settles [10].

ACKNOWLEDGEMENT

A great deal of gratitude is owed to Dr. Luigi Martinelli for his insights and assistance during both the course of this research and the preparation of this paper. The computational and experimental data used for comparison was kindly provided by Dr. Doyle Knight, Dr. Gary Settles, and Prof. Seymour Bogdonoff, and we appreciate their assistance.

REFERENCES

[1] T.J. Mitty, T.J. Baker, and A. Jameson. Generation and adaptive alteration of unstructured three-dimensional meshes. In A.S. Arcilla, J.H. Häuser, P.R. Eiseman, and J.F. Thompson, editors, *Numerical Grid Generation in Computational Fluid Dynamics and Related Fields*, pages 3–12, North-Holland, 1991. Elsevier Science Publishers B.V.

[2] T.J. Baker. Automatic mesh generation for complex three-dimensional regions using a constrained Delaunay triangulation. *Engineering with Computers*, 5:161–175, 1989.

[3] A. Jameson and T.J. Baker. Improvements to the aircraft Euler method. *AIAA paper 87-0452*, AIAA 25th Aerospace Sciences Meeting, Reno, Nevada, January 1987.

[4] R. Löhner. Generation of three-dimensional unstructured grids by the advancing-front method. *AIAA paper 88-0515*, AIAA 26th Aerospace Sciences Meeting, Reno, Nevada, January 1988.

[5] A. Jameson. Time dependent calculations using multigrid, with applications to unsteady flows past airfoils and wings. *AIAA paper 91-1596*, AIAA 10th Computational Fluid Dynamics Conference, Honolulu, Hawaii, June 1991.

[6] D.J. Mavriplis. Three-dimensional unstructured multigrid for the Euler Equations. *AIAA paper 91-1549-CP*, AIAA 10th Computational Fluid Dynamics Conference, Honolulu, Hawaii, June 1991.

[7] G.S. Settles and D.S. Dolling. Swept shock/boundary-layer interactions: Tutorial and update. *AIAA paper 90-0375*, AIAA 28th Aerospace Sciences Meeting, Reno, Nevada, January 1990.

[8] D. Knight and D. Badekas. On the quasi-conical flowfield structure of the swept shock wave-turbulent boundary layer interaction. *AIAA paper 91-1759*, AIAA 22nd Fluid Dynamics, Plasma Dynamics & Lasers Conference, Honolulu, Hawaii, June 1991.

[9] D. Knight, C. Horstman, B. Shapey, and S. Bogdonoff. The flowfield structure of the 3-D shock wave-boundary layer interaction generated by a 20 deg sharp fin at Mach 3. *AIAA paper 86-0343*, AIAA 24th Aerospace Sciences Meeting, Reno, Nevada, January 1986.

[10] F.S. Alvi and G.S. Settles. A physical model of the swept shock/boundary-layer interaction flowfield. *AIAA paper 91-1768*, AIAA 22nd Fluid Dynamics, Plasma Dynamics & Lasers Conference, Honolulu, Hawaii, June 1991.

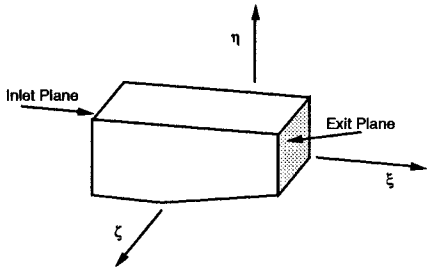

Figure 1: Generic Computational Domain. ($\xi = \frac{x}{\delta_\infty}, \eta = \frac{y}{\delta_\infty}, \zeta = \frac{z}{\delta_\infty}$)

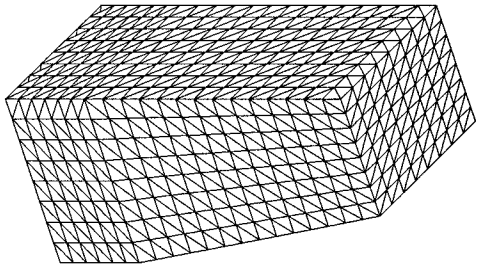

Figure 2: Oblique Shock Wave with Reflection: Initial Mesh Bounding Surface

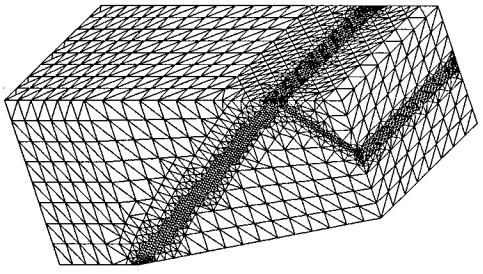

Figure 3: Oblique Shock Wave with Reflection: Adapted Mesh Bounding Surface

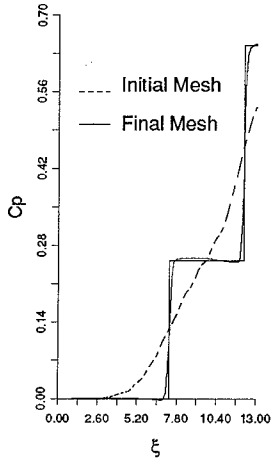

Figure 4: Oblique Shock Wave with Reflection: Pressure Coefficient Distribution (with Theory)

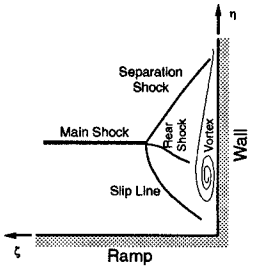

Figure 5: Characteristic Features of the Swept Shock Wave/Boundary Layer Flowfield. ($\eta = \frac{y}{\delta_\infty}, \zeta = \frac{z}{\delta_\infty}$)

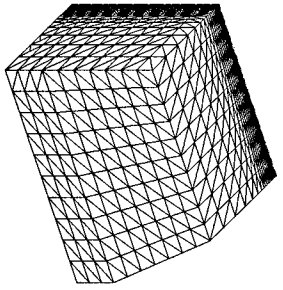

Figure 6: Swept Shock Wave/Boundary Layer Interaction: Initial Mesh Bounding Surface

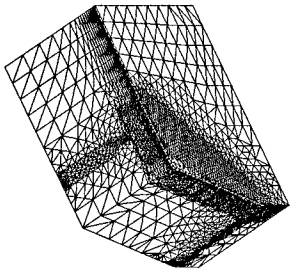

7b: View of Wall, Vortical Sub-Layer, and Ramp Regions

Figure 7: Swept Shock Wave/Boundary Layer Interaction: Final Mesh Bounding Surface

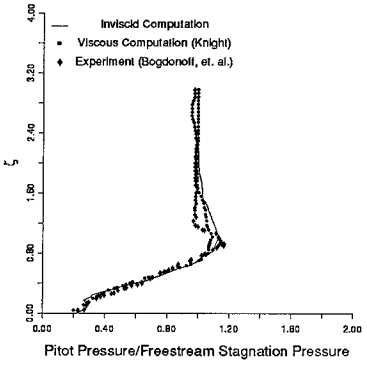

Figure 9: Non-Dimensionalized Pitot-pressure: ($\xi = 4.85, \eta = 5.68$)

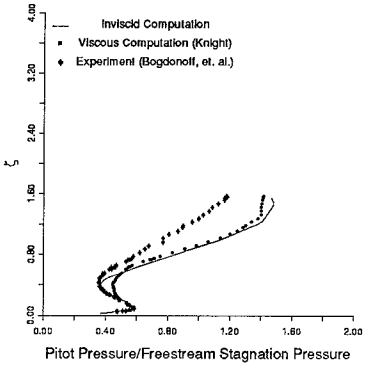

Figure 11: Non-Dimensionalized Pitot-pressure: ($\xi = 6.8, \eta = 5.68$)

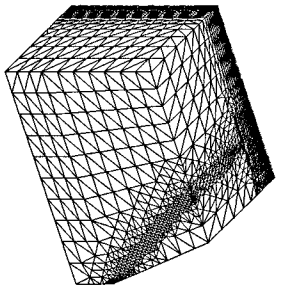

7a: View of Main Shock

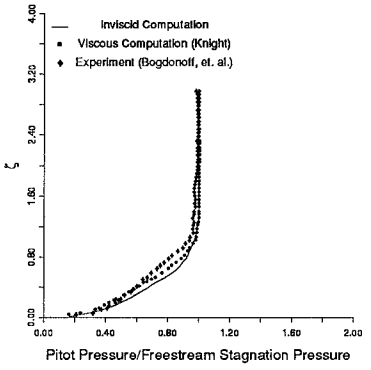

Figure 8: Non-Dimensionalized Pitot-pressure: ($\xi = 1.91, \eta = 5.68$)

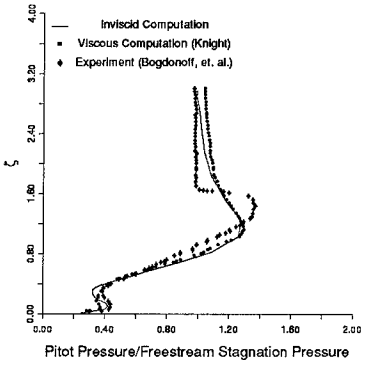

Figure 10: Non-Dimensionalized Pitot-pressure: ($\xi = 5.82, \eta = 5.68$)

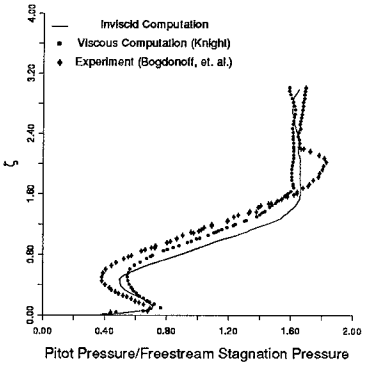

Figure 12: Non-Dimensionalized Pitot-pressure: ($\xi = 7.78, \eta = 5.68$)